Biomass and Bioenergy 217 (2027) 110267

Contents lists available at ScienceDirect

Biomass and Bioenergy

journal homepage: www.elsevier.com/locate/biombioe

European biogenic residues and wastes used for syngas production in a 20 kW_{th} Chemical Looping Gasification unit

J.I. Ruiz Irizar, T. Mendiara, M.T. Izquierdo, L.F. de Diego, F. García-Labiano *

Instituto de Carboquímica, Consejo Superior de Investigaciones Científicas (ICB-CSIC), Miguel Luesma Castán 4, 50018, Zaragoza, Spain

ARTICLE INFO

Keywords:
Chemical looping gasification
Ilmenite
Syngas
Biogenic residues
Biofuels

ABSTRACT

Reaching the targets set by the Paris Agreement demands sustainable alternatives to fossil fuels. Biomass gasification, where syngas is generated and afterwards converted into liquid biofuels, is one of the routes to produce low-carbon fuels. Chemical Looping Gasification (CLG) is a promising route in this context, since the oxygen is supplied to the fuel by a solid oxygen carrier, so that a syngas free of atmospheric N_2 can be obtained without an air separation unit, which simplifies its downstream conversion into biofuels and makes CO_2 capture more feasible. In this work, syngas was generated in a 20 kW_{th} CLG unit from a range of European biomass residues representative of agricultural, forestry, and waste streams, including olive pits, buckwheat pellets, spruce treetops and branches, and waste wood type B, using ilmenite as the oxygen carrier. The process was assessed during about 85 h of steady-state operation. The variables explored were the oxygen-to-fuel ratio, λ, (0.2-0.5), temperature (850-970 °C), and the use of steam or CO_2 as gasifying agent. The oxygen-to-fuel ratio was identified as the most influential variable, with lower values clearly favoring syngas yield, while producing minor differences among the biogenic residues, which had a similar composition. Temperatures above 900 °C enhanced the gasification process, achieving biomass conversions exceeding 90 % for all fuels tested. Carbon emissions to the atmosphere were found to depend on temperature, size and biomass reactivity. The use of CO_2 as gasifying agent enabled the production of syngas with varying H_2/CO molar ratios, which is of interest for its subsequent use in biofuel production.

1. Introduction

Biomass is an essential source of biogenic carbon for sectors that are difficult to decarbonize and cannot be directly electrified, such as aviation and shipping, which require high-density liquid fuels. Biomass provides a more cost-effective renewable carbon option compared to alternatives like electrofuels. Without sufficient biomass, the energy system would increase its costs by around 20 % and would require greater expansion of renewable energy and electrolysis [1]. Therefore, biomass is a crucial and affordable tool for achieving climate goals, provided that its management minimizes emissions and mitigate competition with the food sector.

Biofuels from biomass are usually divided into four generations, depending on the raw material they come from [2]. The first generation uses crops such as sugarcane, maize or rapeseed. They are already produced on a large scale, but they rely on crops that could otherwise be used for food. The second generation, also called advanced biofuels, is obtained from the non-edible parts of plants, mainly farming and forestry residues and other organic wastes. This option valorises materials that would otherwise be discarded and avoids competition with food resources [3]. The third generation comes from algae, which grow quickly and need no farmland, although growing and harvesting them is still expensive [4]. The fourth-generation biofuels use modified microorganisms to capture more carbon, but it is still in the early stages of development [5]. Among these routes, the second-generation biofuels are the most realistic choice today and is close to industrial use. The recently published Renewable Energy Directive III (RED III) points in the same direction [6]. For this reason, advanced biofuels from biogenic residues are the focus of this study.

Organic waste and biomass residues identified for biofuel production in the 2030–2050 period in the EU fall into three categories: agricultural residues, forestry residues and biogenic waste. Agricultural residues come from crops such as cereals, oilseeds, and rice husks. Forestry residues include materials from logging (harvest, tree maintenance) and wood processing. Biogenic waste covers streams such as wood and food waste, paper, municipal solid waste, sewage sludge, and manure [7]. The amounts of these wastes and residues estimated for 2030 range from

* Corresponding author.
E-mail address: glabiano@icb.csic.es (F. García-Labiano).

https://doi.org/10.1016/j.biombioe.2026.110267
Received 3 August 2026; Received in revised form 28 October 2026; Accepted 29 October 2026
Available online 6 November 2026
0961-9534/© 2026 The Authors. Published by Elsevier Ltd. This is an open access article under the CC BY-NC-ND license (http://creativecommons.org/licenses/by-nc-nd/4.0/).

Nomenclature

C_{AR}	carbon emitted in the air reactor (%)
$F_{O2,AR,in}$	Molar flow of O_2 fed into the air reactor (mol/s)
$F_{C,AR,out}$	Molar flow of carbon contained in the gas at the AR outlet (mol/s)
$F_{C,FR,out}$	Molar flow of carbon contained in the gas at the FR outlet (mol/s)
$F_{CO,FR,out}$	Molar flow of CO contained in the gas at the FR outlet (mol/s)
$F_{CH4,FR,out}$	Molar flow of CH_4 contained in the gas at the FR outlet (mol/s)
$F_{H2,FR,out}$	Molar flow of H_2 contained in the gas at the FR outlet (mol/s)
m_o	Oxidised mass of the oxygen carrier in the thermogravimetric analysis (g)
m_r	Reduced mass of the oxygen carrier in the thermogravimetric analysis (g)
$\dot{m}_{sf}$	Mass flow rate of solid fuel (kg/s)
T_{FR}	Fuel reactor temperature (°C)
X_b	Biomass conversion (%)
Y_{sg}	Syngas yield (Nm^3 (H_2+CO)/kg biomass dry basis)
Y_{HC}	Hydrocarbons yield (Nm^3 (C_xH_y)/kg biomass dry basis)
S/CO_2	Steam to CO_2 molar ratio
Symbols	
Ω_{sf}	Oxygen demand for the complete combustion of the biomass (mol O/kg biomass)
λ	Oxygen-to-biomass ratio
λ_{FR}	Oxygen-to-biomass ratio in the fuel reactor
λ_{AR}	Oxygen-to-biomass ratio in the air reactor
Acronyms	
LHV	Lower heating value of biomass (kJ/kg)

300 to 1085 million dry tons/year, and for 2050 they range from 285 to 1240 million dry tons/year. The greatest potential comes from agricultural and forestry residues, with the contribution from other wastes being significantly smaller.

Recent studies point out that although the distribution is not homogeneous among all European countries, most of them have great potential for the production and use of biogenic fuels [8]. Countries with high shares in residues potential are France, Germany, Poland, Spain, Romania and Italy (agricultural) together with Finland and Sweden (forestry) [9,10]. The sustainable potential of these residues and wastes is significant, estimated as at least 10 % (agriculture) and 1.5 % (forestry) of the total EU primary energy use, which is set as 12500 PJ in 2050 [11].

Following the Renewable Energy Directive (RED III), by 2030 advanced biofuels (second and third generation) should represent 5.5 % in the transport sector by 2030 [6]. The production of advanced biofuels relies on diverse conversion technologies, broadly categorized into thermochemical, biochemical, and physicochemical processes. Thermochemical technologies include gasification, hydrothermal liquefaction and pyrolysis. Gasification stands out among the thermochemical routes because of its fuel flexibility. In conventional systems the fuel is partially oxidised with air, oxygen or mixtures with steam, each with drawbacks: air produces nitrogen-diluted syngas, while oxygen requires costly, energy-intensive separation. Dual fluidized bed (DFB) systems, which split combustion and gasification into two reactors, avoid some issues but burn part of the char, releasing CO_2 [12]. Therefore, configurations such as Chemical Looping Gasification (CLG) (see Fig. 1) are gaining attention since they deliver undiluted syngas with better carbon

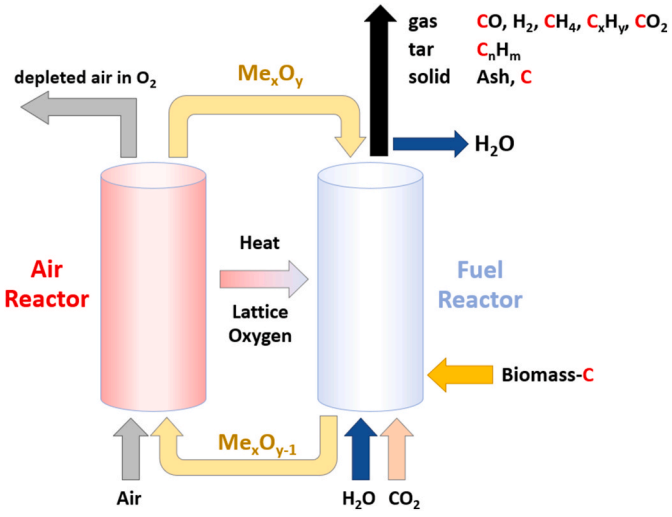


Fig. 1. Scheme of the CLG process.

efficiency and low CO_2 emissions to the atmosphere [13].

In CLG two interconnected fluidized bed reactors are linked by a circulating oxygen carrier, normally a metal oxide. In the FR, biomass is first devolatilized and gasified through reactions (R1) to (R3).

$$Biomass \longrightarrow Volatiles\ (CO, H_2, CH_4, \ldots) + char\ (C) + tar \quad (R1)$$

$$C + H_2O \longrightarrow CO + H_2 \quad (R2)$$

$$C + CO_2 \longrightarrow 2\ CO \quad (R3)$$

The oxygen carrier reacts in parallel with the gas phase composed of volatiles and char gasification products (R4 - R6). The reduced oxygen (Me_xO_{y-1}) carrier is then sent to the air reactor, where exothermic oxidation in air regenerates it and closes the redox loop (R7). The oxidation step provides the sensible heat that sustains the endothermic gasification reactions in the fuel reactor.

$$CH_4 + Me_xO_y \longrightarrow CO + 2H_2 + Me_xO_{y-1} \quad (R4)$$

$$H_2 + Me_xO_y \longrightarrow H_2O + Me_xO_{y-1} \quad (R5)$$

$$CO + Me_xO_y \longrightarrow CO_2 + Me_xO_{y-1} \quad (R6)$$

$$Me_xO_{y-1} + \frac{1}{2}\ O_2 \rightarrow Me_xO_y \quad (R7)$$

The water gas shift reaction (R8) proceeds in parallel to the reactions mentioned above.

$$CO + H_2O \longleftrightarrow CO_2 + H_2 \quad (R8)$$

The air flow fed to the air reactor can also be adjusted so that the system operates under auto-thermal conditions [14,15]. This decoupling between fuel and air, together with the option of reaching negative CO_2 emissions when the process is integrated with carbon capture and storage, is at the core of the interest in CLG. Ever since the technology was first proposed [16], CLG has drawn an increasing interest from the research community, and remarkable progress has been reported over the last years along with the role of CLG within broader bioenergy and carbon-removal strategies [17].

CLG has gained significant operational experience in recent years through a range of continuously operated interconnected fluidized-bed units [18]. In Guangzhou, Wei et al. [19] operated a 10 kW_{th} unit fueled with pine sawdust to evaluate Fe-based oxygen carriers. At Nanjing, Ge et al. [20] investigated CLG at the 25 kW_{th} scale using lignite and rice husk as fuels, demonstrating oxygen-transport control through dilution of hematite-based oxygen carriers with sand. At CSIC,

Condori et al. [21–23] further advanced the technology by demonstrating air reactor (AR) oxygen restriction as a viable process-control strategy in a 20 kW_{th} unit operated with agricultural and forestry residues, including wheat straw, pine forest residue, and torrefied wheat straw. At larger scale, a major milestone was subsequently achieved by TU Darmstadt, which demonstrated stable autothermal CLG operation for more than 400 h in a 1 MW_{th} pilot unit fueled with wood and straw pellets [24,25]. To date, the largest CLG demonstration is the 5 MW_{th} CHEERS unit at Tsinghua University, which has been operated with wood pellets and ilmenite as oxygen carrier [26].

The aim of the present study is to evaluate in a 20 kW_{th} CLG facility the gasification performance and the syngas quality of four representative European second-generation biogenic residues. Different fuel reactor temperatures and oxygen-to-fuel ratios will be evaluated for each biomass, together with the influence of biomass particle size and the steam-to-CO_2 ratio used as the gasifying agent in the fuel reactor. By comparing the results obtained for these fuels under a range of operating conditions, this work aims to provide a basis for optimizing CLG operation and feedstock selection for diverse syngas applications within the European bioeconomy. To the best of our knowledge, the effect of co-feeding CO_2 as gasifying agent in the CLG of biogenic residues has not been studied before in a continuously operated unit at this scale.

2. Experimental

2.1. Oxygen carrier

The ilmenite used as oxygen carrier came from a Norwegian natural ore supplied by Titania AS, with a reported purity of 94.3 %. The mineral is essentially iron titanium oxide and was received in its reduced form, $FeTiO_3$. The raw ore was crushed and sieved to obtain particles in the 100-300 μm range. Particles were pre-oxidised in air at 950 °C for 24 h to improve their mechanical strength. Temperature is the main factor in this step, since it drives the oxidation of $FeTiO_3$ to pseudobrookite, whereas the long time was chosen to ensure that the whole batch was completely oxidised, as in previous works with this ilmenite [21]. XRD analysis of the calcined ilmenite gave the following composition: 54.7 wt% pseudobrookite (Fe_2TiO_5), 11.2 wt% hematite (Fe_2O_3). 28.6 wt% rutile (TiO_2), together with about 5.5 wt% of other inert compounds. Table 1 summarizes the main properties of the calcined ilmenite and after operation.

The oxygen transport capacity of ilmenite (R_{OC}) is defined as the fraction oxygen in the oxygen carrier that can be transferred and it was determined by thermogravimetric analysis (15 vol % H_2 at 950 °C in TGA).

$$R_{OC} = \frac{m\text{-}m_r}{m_o} \quad (1)$$

After the campaign, the oxygen transport capacity of the ilmenite was practically unchanged (3.9 % compared with 4.0 %), whereas its porosity and BET surface area increased and its crushing strength decreased (Table 1), as is typical of the ilmenite behavior during redox cycles. Some deposition of ash-forming elements, mainly Na, K, P and Ca, was found on the used particles, but it did not affect their oxygen transport capacity. No particle sintering or agglomeration, or carbon deposition, was observed after operation.

Table 1
Physical properties of the calcined ilmenite and after operation.

	Calcined	Post operation
Oxygen transport capacity, R_{OC} (%)	4.0	3.9
Skeletal density (kg/m^3)	4100	3700
Crushing strength (N)	2.2	1.1
Porosity (%)	1.2	33.7
BET surface area (m^2/g)	0.8	32.7

2.2. Biogenic residues

Four EU biogenic residues were selected to represent three distinct residue streams: waste wood (waste wood type-B), agricultural residues (olive stones and buckwheat husk), and forestry residues (spruce treetops and branches). The biogenic residues were selected based on their availability at the European level, taking into account sufficient production volumes and the seasonality constraints that could affect their supply. Recent data of annual primary production for olive and buckwheat was retrieved from FAOSTAT, and coniferous roundwood removals and wood-waste generation from Eurostat. These figures were translated into the corresponding residue streams by conversion factors reported [27–29]. For the period 2014-2024, the EU annual mass production for waste wood-B, olive stone and buckwheat husk was around 900, 2.5 and 0.05 Mt/year, respectively. The main reasons for the low production in agricultural residues are their seasonal production and the territorial dispersion of producers [30,31]. On the other side, the EU annual volume production in the same 2014-2024 period of spruce and pine residues was around 300-350 Mm^3/year.

Another characteristic from biomass to consider is the physical form of the different biogenic residues, (see Fig. 2). Waste wood-B and buckwheat husk were supplied in pelletized form to increase fuel density, and facilitate transport and handling. Both fuels were initially tested as received (20-30 mm in length), but these long pellets occasionally caused discontinuities in the fuel feeding and fluctuations in the gas composition. For this reason, both fuels were subsequently crushed to a smaller size (≈10 mm), ensuring continuous fuel feeding and stable operation of the unit. It should also be noted that spruce and olive stone have different shapes. Spruce residues are more heterogeneous and needle- or splinter-shaped, whereas olive pit residues are more homogeneous and rounded. Olive stone and spruce were fed as received, since their size was already suitable for the screw feeder, and their feeding was continuous and smooth in all the tests. Despite crushing, the pellets remained larger than most olive stone and spruce particles, so particle size and type of residue are partly linked in this study. Tests 1.1-1.10 (WWB) and 3.1-3.4 (BW) were carried out with the pellets as received (20-30 mm in length), and tests 1.11-1.15 (WWB) and 3.5-3.13 (BW) with the crushed pellets (10 mm), as indicated in Table S1.

Table 2 summarizes the particle size, proximate, ultimate analyses and lower heating value of the four residues used in the CLG unit.

2.3. Experimental setup

The experimental campaign was performed in a Chemical Looping Gasification (CLG) facility consisting of two interconnected circulating fluidized bed reactors that act as fuel and air reactors, respectively, designed for a nominal thermal input of 20 kW_{th} with solid fuels. Fig. 3 shows the configuration of the unit, which is installed at the Instituto de Carboquímica (ICB-CSIC). A detailed description was already given in a previous work, so only the main features are mentioned here [21].

Biomass is fed to the fuel reactor through a double screw feeder. The fuel fall by gravity from the hopper into a slow screw-feeder, whose speed is adjusted to set the biomass mass flow rate delivered to a fast screw-feeder that conveys it into the reactor. Steam and/or CO_2 are used as gasifying agent in the FR and air is supplied to the AR. Dedicated mass flow meters were used to control the gas and liquid feed rates. The loop seals avoid mixing atmospheres between the fluidized bed reactors and balance pressure differences between the interconnected reactors. The loop seals were fluidized with N_2 (2000 NL/h), part of which exited the unit with the fuel reactor gas. Since steam would be used for loop seal fluidization in an industrial-scale unit, syngas compositions are reported on a N_2-free basis.

The double loop seal allows independent regulation of solids circulation, enabling operation either within the internal FR loop or across the AR–FR circulation loop. The tests showed here were carried out without using the internal circulation in the FR. The facility offers also

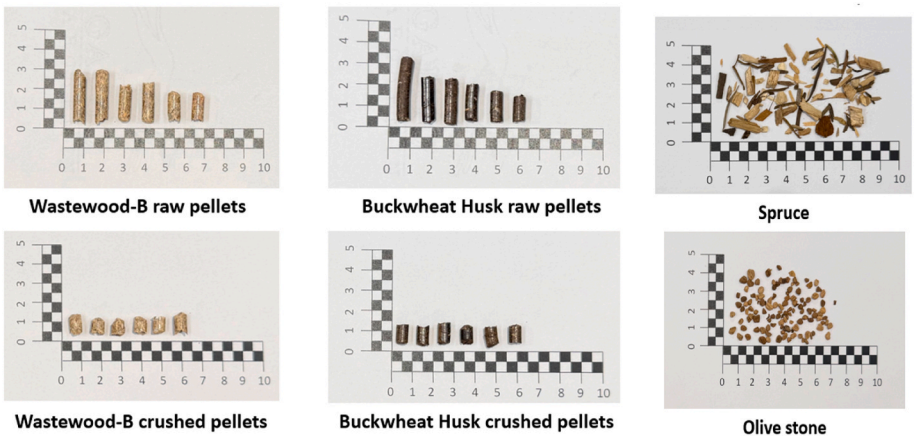


Fig. 2. Size of the biogenic residues used in the experimental campaign in the 20 kW_{th} unit.

Table 2
Size and composition of the biogenic residues and wastes.

Type	Waste Wood	Agricultural residue		Forestry residue
Fuel	Waste Wood Type B	Olive Stone	Buckwheat husk	Spruce
	WWB	OS	BW	SP
Shape	pellets	spherical	pellets	chips
Size raw biomass (mm)	L:20-30, Ø:6	0.5-3.2	L:20-30, Ø:6	0.5-10
Size crushed biomass (mm)	L: 10, Ø:6	-	L: 10, Ø:6	-
Particle density (kg/m^3)	904	1363	1254	410
Proximate analysis				
Moisture	6.8	7.3	8.8	7.9
Ashes	1.7	0.3	1.5	2.5
Volatiles	74.2	74.9	66.4	72.1
Fixed carbon (by dif.)	17.3	17.5	23.3	17.5
Ultimate analysis				
C	46.3	47.8	45.9	46.7
H[a]	5.5	5.3	5.1	5.4
N	1.1	0.2	0.5	0.4
S	0.03	0.04	0.04	0.04
O (by dif.)	38.6	39.0	38.2	37.0
LHV (kJ/kg)	17957	17352	16627	16808

[a] H does not include hydrogen in H_2O.

the possibility to directly measure the solids flux leaving each reactor through diverting valves placed below the cyclones. The solids circulation rate was measured in this way once a day and was assumed to be the same for all the tests carried out that day (see Table S1). The gas flows fed to both reactors were kept constant in all the tests (20000 NL/h of air and N_2 in the air reactor and 5000 NL/h of steam and/or CO_2 together with 3000 LN/h of N_2 in the fuel reactor), which gave superficial gas velocities of 4.4-4.7 m/s in the air reactor and 0.8-2.4 m/s in the fuel reactor depending on the temperature and the gas generated from the biomass. Electrical furnaces were kept on throughout all tests to compensate for heat losses from the unit. Consequently, the unit did not operate under autothermal conditions. However, this approach ensured perfect temperature control and enabled a more reliable assessment of the effects of the different operating conditions.

The outlet gas composition of both reactors is monitored on-line: CH_4, CO and CO_2 are measured by infrared analyzers (Siemens Ultramat 23), H_2 concentration is analyzed by thermal conductivity (Siemens Calomat 6) and O_2 concentration is measured by a paramagnetic analyzer (Siemens Ultramat-Oxymat 6). According to the manufacturer, the linearity deviation and the repeatability of these analysers are within 1 % of the measuring range, and the gas flows fed to the unit were set by

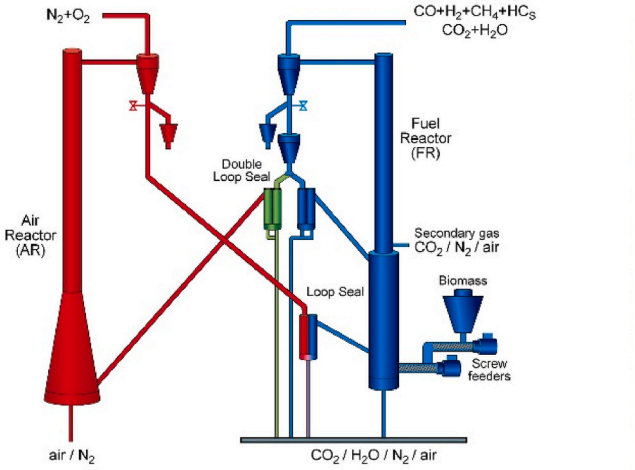


Fig. 3. Layout of the 20 kW_{th} CLG unit at the Instituto de Carboquímica (ICB-CSIC).

mass flow controllers with an accuracy of about 1 % of full scale. The fuel reactor outlet stream is additionally analyzed by gas chromatography to determine the C_2-C_3 content in the FR stream.

The facility operates with an oxygen carrier inventory of approximately 35 kg without continuous solids make-up or purge. To ensure that the same batch of oxygen carrier was used throughout the campaign, 45 kg of calcined ilmenite were initially prepared and circulated in the unit at high temperature for 7 h. Subsequently, 35 kg were maintained into the unit to establish the required solids inventory, while the remaining ilmenite was kept aside for replenishment. At the end of each operating day, the solids collected in the cyclones of the air and fuel reactors were sieved, and particles smaller than 100 μm were discarded. The resulting solids losses were replenished the following day using the reserved ilmenite from the initially prepared batch, thereby maintaining the inventory at approximately 35 kg. In total, ≈3.5 kg of calcined ilmenite was added during the campaign to compensate for these losses.

2.4. Data evaluation

The experimental data analysis enables the evaluation of the efficiency of the CLG process and the effects of different operating conditions.

The oxygen-to-fuel ratio (λ) is defined as the fraction of oxygen fed to the air reactor with respect to the stoichiometric oxygen required for the complete combustion of the biomass.

$$\lambda = \frac{F_{O2,AR,in}}{\dot{m}_{sf} \cdot \Omega_{sf}} \tag{2}$$

where Ω_{sf} is the oxygen demand required to completely burn all the biomass (mol O/kg biomass)

$$\Omega_{sf} = \left(x_C \frac{32}{12} + x_H \frac{16}{2} + x_S \frac{32}{32} - x_O \right) \frac{1000}{16} \tag{3}$$

In this work the oxygen-to-fuel ratio was fixed by controlling the oxygen fed to the air reactor, which was transferred by the oxygen carrier in the fuel reactor [15]. The air reactor was fed with a mixture of air and N_2 at a constant total flow rate, while the O_2 concentration at the inlet was varied with λ, ranging from 3.5 to 6.9 vol%. The O_2 concentration at the air reactor outlet was zero in all the tests, indicating that all the oxygen fed was taken up by the oxygen carrier or used for char combustion, which is one of the main advantages of this method of controlling λ [15]. With this method, the total gas flow in the air reactor, the solids circulation rate and the biomass fed were maintained constant for the different oxygen-to-fuel ratios. Thus, fluid dynamic conditions were kept constant, allowing a better comparison among tests.

The oxygen-to-fuel ratio in fuel reactor (λ_{FR}) is the fraction of oxygen effectively delivered from the oxygen carrier to the fuel in the fuel reactor. It is calculated from the flows of the oxygen-containing compounds at the inlet and outlet of the fuel reactor, $F_{O2,sf}$ being the oxygen contained in the biomass fed, expressed as O_2:

$$\lambda_{FR} = M_{O2} \cdot \frac{\left[\left(F_{CO2,FR,out} + \frac{1}{2} F_{CO,FR,out} + \frac{1}{2} F_{H2O,FR,out} \right) - \left(F_{CO2,FR,in} + \frac{1}{2} F_{H2O,FR,in} + F_{O2,sf} \right) \right]}{\dot{m}_{sf} \cdot \Omega_{sf}} \tag{4}$$

The oxygen-to-fuel ratio in the air reactor (λ_{AR}) is the fraction of the oxygen fed to the air reactor that is taken up by the oxygen carrier, i.e., the oxygen fed minus the oxygen leaving the air reactor as CO_2 by char combustion. It is obtained from an oxygen balance in the air reactor.

$$\lambda_{AR} = M_{O2} \cdot \frac{\left(F_{O2,AR,in} - F_{CO2,AR,out} \right)}{\dot{m}_{sf} \cdot \Omega_{sf}} \tag{5}$$

In steady state, all the oxygen taken up by the oxygen carrier in the air reactor is released to the fuel in the fuel reactor, so λ_{AR} and λ_{FR}, which are calculated from independent balances, should be equal.

Regarding to the key performance parameters, the biomass conversion (X_b) is the amount of carbon contained in the biomass that is converted into gas, both in the FR and AR.

$$X_b = \frac{\left(F_{C,FR,out} + F_{C,AR,out} \right)}{F_{C,b}} \tag{6}$$

The rest of the carbon fed not converted to gas, that is $(100 - X_b)$, corresponds to elutriated char and tar.

The carbon emitted in AR (C_{AR}) is the percentage of carbon converted to gas in the AR in relation to the total carbon converted in the system.

$$C_{AR} = \frac{F_{C,AR,out}}{F_{C,FR,out} + F_{C,AR,out}} \tag{7}$$

The syngas yield (Y_{sg}) represents the amount of H_2 and CO generated in the FR in relation to the biomass fed into the system, expressed in Nm^3/kg dry biomass:

$$Y_{sg} = Y_{H2} + Y_{CO} = \frac{G_{H2}}{\dot{m}_{sf}} + \frac{G_{CO}}{\dot{m}_{sf}} \tag{8}$$

In a similar way, the hydrocarbons yield represents the amount of CH_4 and C_xH_y generated in the FR in relation to the biomass fed into the system, expressed in Nm^3/kg dry biomass

$$Y_{HC} = \frac{F_{CH4,FR,out} + \sum F_{CxHy,FR,out}}{\dot{m}_{sf}} \tag{9}$$

3. Results and discussion

The experimental campaign was designed to evaluate the potential of the four biogenic residues in the production of syngas and assess the influence of the main CLG operating variables on the quality of the syngas obtained. The evolution of the temperatures, gas concentrations and pressure drops of the fuel and air reactors during a whole day of operation with spruce is shown as an example in Fig. S1 of the Supplementary Material. The operation was stable with all the residues.

About 85 h of steady-state operation were accumulated while three variables were systematically modified: fuel reactor temperature (T_{FR} = 850-970 °C), oxygen-to-fuel ratio (λ = 0.20-0.50) and the composition of the gasifying agent with four steam-to-CO_2 ratios, S/CO_2, (25/75, 50/50, 75/25, and 100/0). A comprehensive table (Table S1) summarizing all the results for the four biogenic residues is supplied as Supplementary Material. All data plotted in Figs. 4–14 correspond to tests listed in Table S1. Each test corresponds to a single steady-state period, which lasted between 0.5 and 5.75 h, and the values given are averages over that period. To determine repeatability, instead of

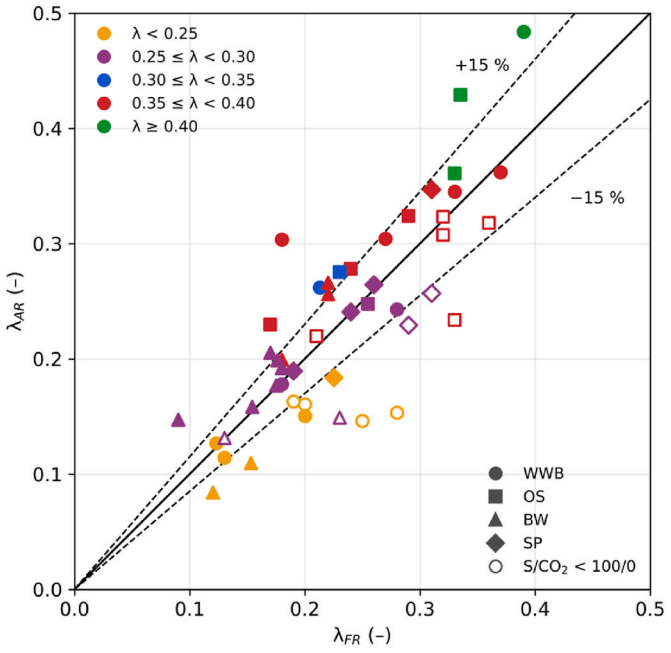


Fig. 4. Oxygen-to-fuel ratio in the air reactor (λ_{AR}) versus that in the fuel reactor (λ_{FR}) for all the tests. Solid line: $\lambda_{AR} = \lambda_{FR}$; dashed lines: ±15 %.

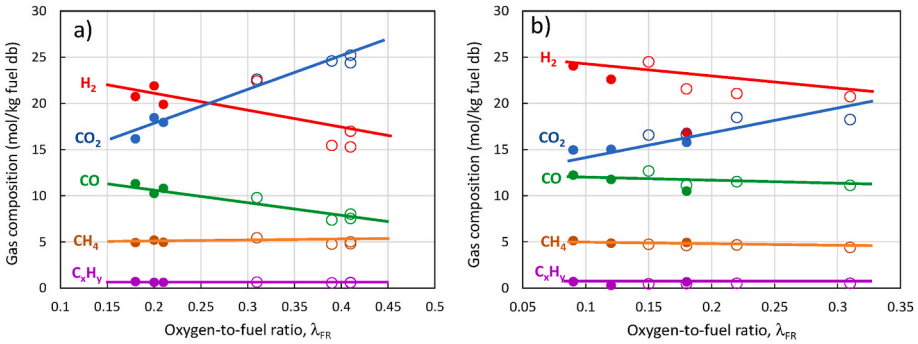


Fig. 5. Effect of the oxygen-to-fuel ratio, λ_{FR}, on the molar composition of the fuel reactor outlet gas for (a) waste wood type B (WWB) and (b) buckwheat pellets (BW) at $T_{FR} = 950\,°C$ and $S/CO_2 = 100/0$. Open and filled symbols correspond to pellets with 10 mm and 20-30 mm length, respectively.

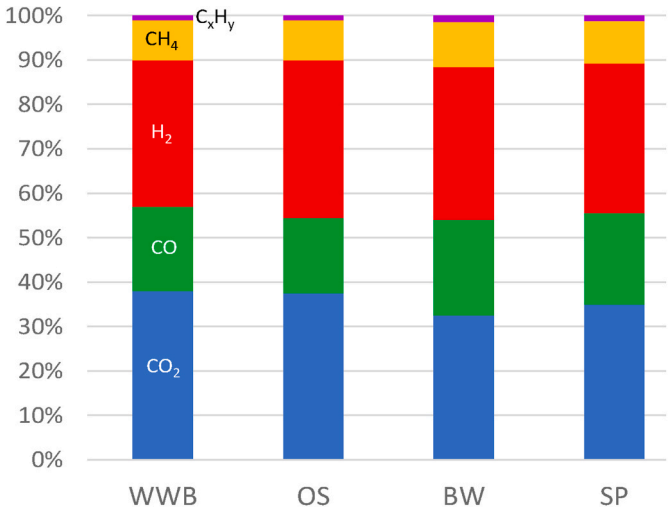


Fig. 6. Gas composition (vol% d.b.) at the reference λ for autothermal operation for the four biogenic residues (λ~0.30-0.35, steam 100 %) at $T_{FR} = 950\,°C$.

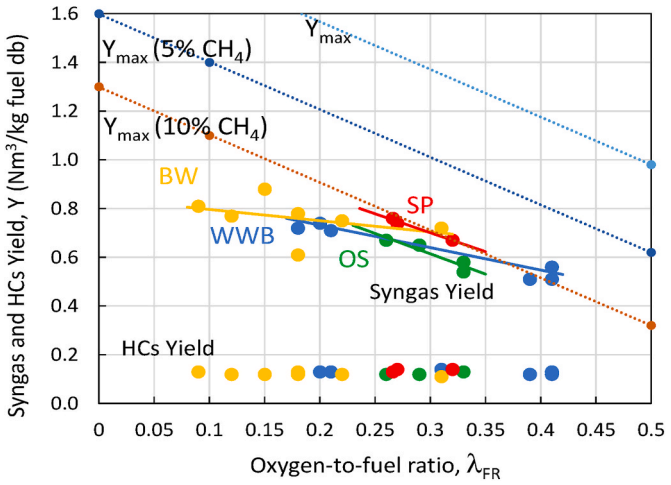


Fig. 8. Effect of the oxygen-to-fuel ratio in the fuel reactor, λ_{FR}, on the syngas yield and hydrocarbon yield for the four biogenic residues. Conditions: $T_{FR} = 950\,°C$, $S/CO_2 = 100/0$.

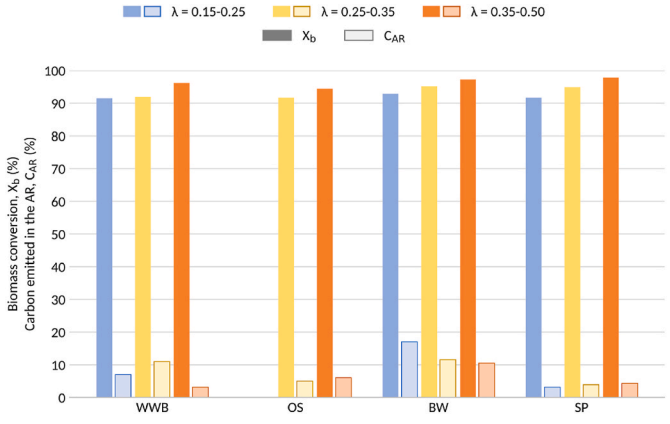


Fig. 7. Biomass conversion (X_b, dark bars) and carbon emitted in the air reactor (C_{AR}, light bars) for the four biogenic residues at three ranges of λ. $T_{FR} \approx 950\,°C$, $S/CO_2 = 100/0$). WWB and BW: crushed pellets (10 mm).

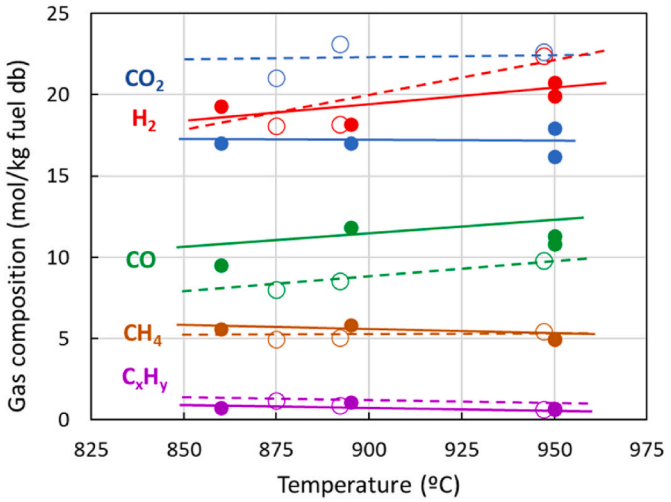


Fig. 9. Effect of the fuel reactor temperature, T_{FR}, on the syngas composition for waste wood type B (WWB) at λ ~0.3 and $S/CO_2 = 100/0$. Open and filled symbols correspond to pellets with 10 mm and 20–30 mm length, respectively.

repeating the same conditions several times, one operating variable was changed at a time while the rest were kept constant, so that each trend is defined by several tests. A test was considered to be in steady state when all the operating conditions (fuel feed, gas flows to both reactors) had been kept constant and the temperatures, pressure drops and gas concentrations at the outlet of both reactors showed no drift. Under these conditions, the oxidation degree of the oxygen carrier did not change, and the oxygen taken up in the air reactor (λ_{AR}) should be equal to that transferred to the fuel in the fuel reactor (λ_{FR}). The comparison between both values in Fig. 4 shows that they were distributed around the diagonal for all the biogenic residues, with the ±15 % deviation lines

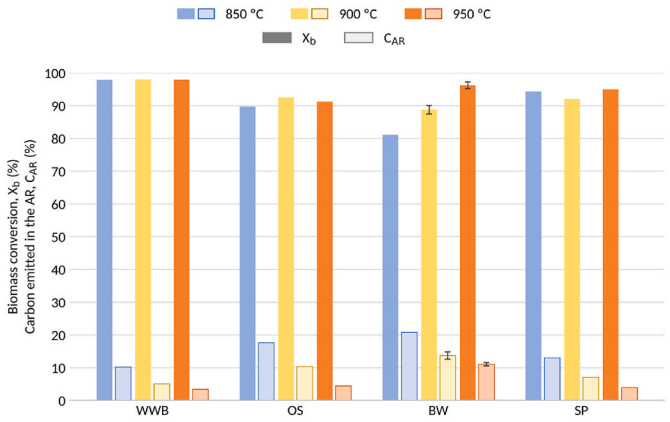


Fig. 10. Effect of the fuel reactor temperature on the biomass conversion (X_b, dark bars) and the carbon emitted in the air reactor (C_{AR}, light bars) for the four biogenic residues (λ = 0.27-0.38, S/CO_2 = 100/0). WWB and BW: crushed pellets (10 mm).

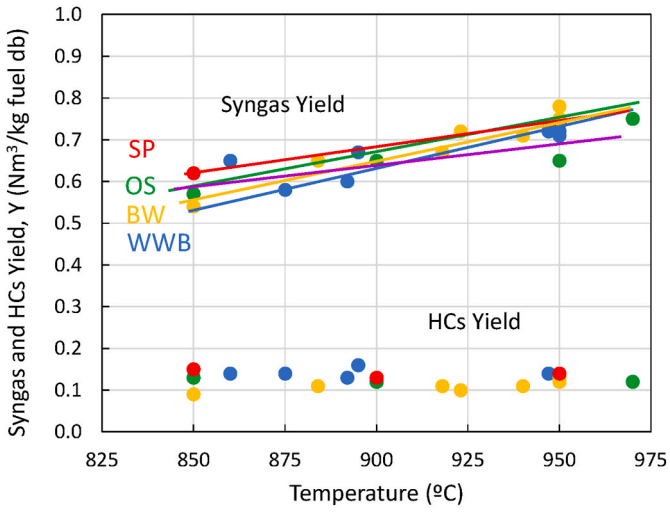


Fig. 11. Effect of the fuel reactor temperature on the syngas yield and hydrocarbon yield for the four biogenic residues. Conditions: λ ~0.3, S/CO_2 = 100/0. Buckwheat husk and waste wood type B are shown for the crushed 10 mm pellets.

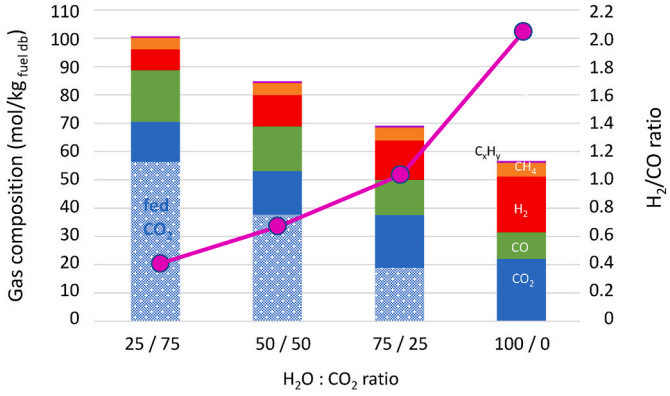


Fig. 12. Effect of the steam-to-CO_2 ratio on the molar composition of the fuel reactor outlet gas for olive stone (OS) at T_{FR} = 950 °C and λ = 0.36.

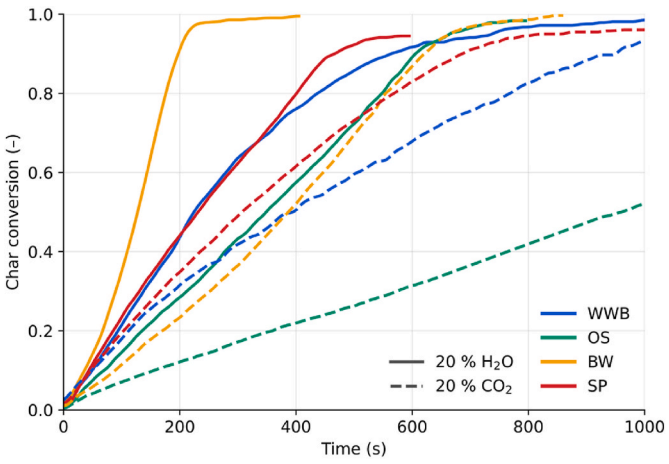


Fig. 13. Char conversion versus time for the gasification of the four biogenic residues at 900 °C with 20 % steam (solid lines) and 20 % CO_2 (dashed lines).

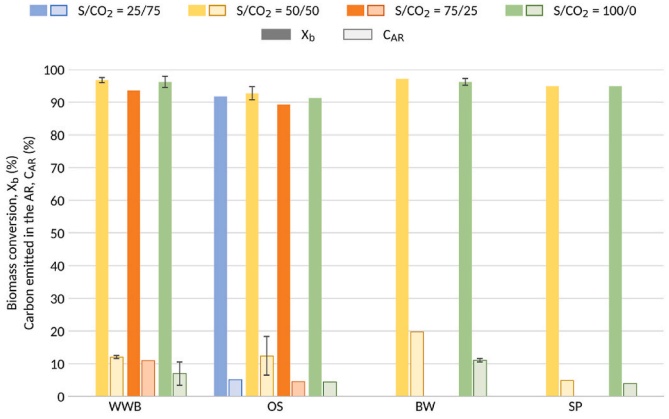


Fig. 14. Effect of the steam-to-CO_2 ratio on the biomass conversion (X_b, dark bars) and the carbon emitted in the air reactor (C_{AR}, light bars) for the four biogenic residues. Conditions: λ ~0.3, T_{FR} = 950 °C.

shown as reference. The largest deviations corresponded to tests with steam-CO_2 mixtures, for which λ_{AR} was generally lower than λ_{FR} because the large CO_2 flow fed makes the oxygen balance in the fuel reactor less precise.

3.1. *Effect of the operating parameters*

3.1.1. *Effect of the oxygen-to-fuel ratio (λ)*

The oxygen-to-fuel ratio (λ) is known to be the main operating variable controlling the CLG process [21]. The four biogenic residues were tested using different values of this parameter and results obtained followed the same trends, with small differences in the absolute values reached. As an example, Fig. 5 shows the molar composition of the gas leaving the fuel reactor as a function of λ_{FR} for waste wood type B (WWB) and buckwheat (BW). In the graph, two sizes of pellets are considered: pellets as received (20-30 mm) and crushed pellets (10 mm). For both sizes, an increase in λ_{FR} produced an increase in the CO_2 flow (and also in H_2O) and a decrease in the H_2 and CO generated. This effect of λ_{FR} is linked to the higher lattice oxygen available for reaction inside the fuel reactor as the λ_{FR} values increase. It is remarkable the high amount of CH_4 found and the presence of small amounts of C_2-C_3 hydrocarbons (C_xH_y in the graph). The CH_4 content in all these tests were between 8 and 12 vol%, which is similar to the reported in previous CLG

studies [21–25]. CH_4 is mainly released during the devolatilisation of the biomass, and it is hardly converted afterwards because of the poor contact between the volatile plumes and the oxygen carrier in the bed and riser, as well as the low reactivity of ilmenite towards CH_4 [32,33].

Samprón et al. [15] estimated that the oxygen-to-fuel ratio to reach autothermal operation in CLG processes was about 0.30-0.35, depending on the C_1-C_5 hydrocarbons released [15]. Since the 20 kW_{th} unit is electrically heated, autothermal operation was not demonstrated in this work. Instead, the CLG process was investigated over a range of λ. Therefore, the four biogenic residues were compared under theoretically autothermal conditions, λ ≈ 0.30-0.35. Fig. 6 compares the gas composition obtained from the experimental data at this reference range considering results for crushed pellets (10 mm) in the case of both waste wood B (WWB) and buckwheat pellets (BW). It can be seen that gas composition was very similar for all the fuels, which means that the syngas produced depends more on the oxygen-to-fuel ratio, than on the fuel used or, in this case, the type of biogenic residue, i.e. agricultural, forestry or waste wood. Therefore, under theoretical autothermal conditions, λ ≈ 0.30-0.35, the expected syngas composition for any biogenic residue would be approximately 35 % H_2, 19 % CO, 36 % CO_2, 9 % CH_4, and 1 % C_2-C_3 hydrocarbons.

In addition to the syngas composition, the effect of the type of the biogenic residue used on the key performance indicators was analyzed. Fig. 7 presents the total biomass conversion (X_b) and the carbon emitted in the AR (C_{AR}) for the four biogenic residues tested and at different range values of λ.

Regarding biomass conversion, values above 90 % were obtained for all biogenic residues regardless the oxygen-to-fuel ratio. At 950 °C, the carbon emitted in the air reactor (C_{AR}) was below 6.5 % for spruce (SP) and olive stone (OS). For the pellets, C_{AR} for 10-mm WWB and BW pellets (shown in Fig. 7), was 3.4 % and 11.5 %, respectively. For the whole pellets, C_{AR} larger values were obtained under the same conditions, i.e., 11 % and 21.2 %, respectively. It has to be indicated that the 20 kW_{th} unit has no carbon stripper to improve fuel conversion because it was not effective with pelletized biomass [21].

Finally, Fig. 8 presents the effect of oxygen-to-fuel ratio on the syngas yield, Y_{sg}, and the hydrocarbon yield, $Y_{HC's}$ for the four biogenic residues, together with the theoretical maximum syngas yield, $Y_{max,}$ as a function of the CH_4 content. The syngas yield decreased when increasing the oxygen-to-fuel ratio, λ_{FR}, for all the types of biomass tested. In contrast, hydrocarbon yield was not affected by this parameter. However, no significant differences were observed among the four biogenic residues in terms of values obtained. On average, at λ ≈ 0.30-0.35, the range estimated for autothermal operation [15], a syngas yield, Y_{sg}, of approximately 0.7 Nm^3/kg biomass d.b. and a hydrocarbon yield, $Y_{HC's}$, of 0.15 Nm^3/kg biomass d.b. can be expected for these biogenic residues. The theoretical limit, $Y_{max,}$ plotted corresponds to the syngas yield that would be obtained if the methane leaving the fuel reactor was fully reformed to CO + $3H_2$. Thus, considering the experimental data, since the outlet CH_4 remains almost constant with λ, it is confirmed that the decline of Y_{sg} with λ is governed by the over-oxidation of H_2 and CO to H_2O and CO_2 rather than by the presence of methane or higher hydrocarbons. Therefore, the conversion of these compounds into syngas could produce a high increase in the syngas yield. This could be done with the use of oxygen carriers with catalytic activity regarding hydrocarbons reforming [34] or by new reactor designs improving the contact between the oxygen carrier and volatiles [35].

3.1.2. Effect of the fuel reactor temperature

The effect of the fuel reactor temperature (T_{FR}) on the gasification of the four biogenic residues was investigated, as temperature strongly influences kinetics of the endothermic char gasification reactions (R2 and R3). Its effect was studied between 850 and 950 °C for the four biogenic residues at a fixed oxygen-to-fuel ratio (λ ~ 0.3) and pure steam as gasifying agent. In this analysis, waste wood type B was taken as the representative residue to describe the effects of temperature on syngas composition. Fig. 9 shows the molar composition of the fuel reactor outlet gas as a function of T_{FR} for the two sizes of the WWB pellets.

In contrast with the strong response found for the oxygen-to-fuel ratio (Fig. 5), the syngas composition was only weakly affected by temperature, confirming that the syngas composition is governed primarily by λ rather than by the fuel reactor temperature, T_{FR}. The hydrocarbons behaved similarly, as CH_4 and the C_2–C_3 fraction remained practically constant with temperature. Nevertheless, although the relative composition changed little, the amounts of H_2 and CO produced increased with temperature, because the faster steam–char gasification (R2) converted a larger fraction of the fixed carbon into permanent gas. The effect of the biomass particle size can be analyzed with the two pellet lengths tested for WWB and BW (Figs. 5 and 9). Shortening the pellets from 20-30 mm to 10 mm produced a more oxidised gas, with higher CO_2 and lower CO and H_2. This was attributed to enhanced heat transfer and gasifying-agent access to the char, which promoted char gasification in the fuel reactor and reduced char transfer to the air reactor (lower C_{AR}). Consequently, more oxygen from the air reactor was taken up by the oxygen carrier rather than consumed by char combustion, increasing its oxidation state and promoting further oxidation of CO and H_2 to CO_2 and H_2O. This is consistent with the higher λ_{FR} values observed for the crushed pellets at similar λ (Table S1): 0.28 vs. 0.18 for WWB and 0.18 vs. 0.09 for BW. However, smaller particles may be more easily elutriated, reducing their residence time and increasing unconverted char losses. The presence of CH_4 and C_2-C_3 in the syngas was hardly affected by the particle size of the pellets.

Fig. 10 shows the total biomass conversion (X_b) for the four biogenic residues and the carbon emitted in the air reactor (C_{AR}) at 850, 900 and 950 °C, considering, for WWB and BW, the crushed 10 mm pellets. The biomass conversion was over 90 % in almost all cases. A pronounced increase with temperature was observed for buckwheat husk (BW), which was the least converted residue at the lowest temperature, in agreement with the faster steam-char gasification at higher temperature. At the highest temperature tested (950 °C), the carbon emitted in the air reactor was below 5 % for WWB (crushed pellets), OS and SP, whereas it was about 11 % for BW (Fig. 10). For WWB, the crushed pellets gave much lower C_{AR} values than the whole pellets at 900 and 950 °C (3.4-5.1 % compared with 10.5-17.8 %), whereas at 850 °C both sizes gave a similar value (about 10 %) (Table S1). The C_{AR} values decreased with increasing temperature for all fuels, which can be attributed to the enhanced gasification of char at higher T_{FR} temperatures. Under these conditions, a larger fraction of the carbon was converted into gaseous species in the FR, thereby reducing the amount of carbon transferred to the air reactor for subsequent combustion and emission.

Finally, the effect of the fuel reactor temperature on the syngas and hydrocarbon yield (Y_{sg} and Y_{HC}) was investigated in Fig. 11 for the four biogenic residues at λ ~0.3 and steam gasification, also considering results for the crushed 10 mm pellets when corresponding. The syngas yield increased steadily with temperature, since the endothermic char gasification (R2 and R3) converted a larger fraction of the fixed carbon into H_2 and CO, so that the chemical energy recovered in the syngas grows accordingly. Again, no relevant differences between biogenic residues were observed. Regardless the origin of the residue (agricultural, forestry or waste wood), the maximum value of the syngas yield reached at 950 °C was close to 0.7 Nm^3/kg biomass d.b.

3.2. Effect of the gasifying agent

Among the various gasifying agents used in biomass gasification, steam and carbon dioxide (CO_2) are the most common, since they promote different gasification reactions and lead to different syngas compositions and process performances. The influence of the gasifying agent was examined in the 20 kW_{th} CLG unit by feeding the fuel reactor with steam-CO_2 mixtures of different composition. Four steam-to-CO_2 ratios (S/CO_2 = 25/75, 50/50, 75/25 and 100/0) were tested at a constant fuel reactor temperature (T_{FR} = 950 °C) and oxygen-to-fuel ratio (λ ~ 0.3).

Fig. 12 shows the molar composition of the fuel reactor outlet gas for olive stone (OS) as a function of the steam fraction in the gasifying agent. To improve the clarity of the results, the CO_2 introduced into the system is plotted separately (lower segment) from the CO_2 generated in the fuel reactor. As the S/CO_2 ratio decreased from 100/0 to 25/75, the amount of CO_2 generated decreased steeply, whereas the CO produced grew moderately, from 10 to 18 mol/kg dry biomass. This indicates that only a small fraction of the additional CO_2 supplied as gasifying agent was converted into CO via the Boudouard reaction (R3), while most of the fed CO_2 left the fuel reactor unreacted. Taking the steam-only test as reference, only 14-18 % of the CO_2 fed was converted, and the increase in CO (3.0-8.8 mol/kg dry biomass) was close to the CO_2 consumed (3.4-8.0 mol/kg dry biomass). As a result, most of the CO_2 leaving the fuel reactor was CO_2 that had been fed (about 80 % at S/CO_2 = 25/75), and most of the change in syngas composition is due to dilution by unreacted CO_2 rather than to a change in the gasification chemistry. Since the gas-solid contact in the bed is the same with both gasifying agents, the differences found between steam and CO_2 come mainly from their different reactivity with the char. In contrast, the H_2 yield decreased significantly as the steam content in the gasifying agent was reduced, owing to the lower contribution of steam-char gasification (R2) and the water-gas shift reaction (R8). Consequently, the H_2/CO ratio increased markedly with increasing steam fraction in the gasifying agent.

Overall, the choice of gasifying agent depends on the intended application. Steam maximises the H_2 yield and the H_2/CO ratio, which is convenient for hydrogen-rich syntheses such as methanol production. Feeding CO_2 lowers the H_2/CO ratio and could be considered when a CO-richer syngas is required or when captured CO_2 is available on site, always taking into account its lower reactivity. With steam alone, the H_2/CO ratio was about 1.6-2.3 (Table S1), close to the value of about 2 needed for methanol synthesis or Co-based Fischer-Tropsch synthesis, whereas the S/CO_2 = 50/50 mixtures gave H_2/CO ratios of about 0.7-1.0, which are more suitable for Fe-based Fischer-Tropsch synthesis or direct DME synthesis. For methanol production, steam is therefore the most suitable gasifying agent, and CO_2 co-feeding would only be useful for small adjustments of the H_2/CO ratio, at the cost of a lower carbon conversion in the fuel reactor.

To test the intrinsic reactivity of the biogenic residues regarding the gasifying agent, char from all of them was prepared in a batch fluidized bed reactor at 900 °C and subsequently tested in TGA. The thermogravimetric experiments were done at 900 °C with 20 % steam or 20 % CO_2 in a nitrogen flow. Fig. 13 shows the corresponding char conversion vs. time curves obtained under those conditions.

The reactivity of the chars was higher using steam than CO_2 as gasifying agent. The influence of the gasifying agent is especially significant in the case of the buckwheat pellets and olive stones, whose reactivity with CO_2 experiences an important decrease when compared to steam. It can be also seen that the char from olive stones is the least reactive of all those tested.

The effect of S/CO_2 ratio on the total biomass conversion and carbon emitted in the AR (C_{AR}) is shown in Fig. 14 for the four biogenic residues tested. No clear trend was observed in biomass conversion as a function of the gasifying-agent composition. However, the amount of carbon emitted from the air reactor appeared to decrease with increasing S/CO_2 ratio, suggesting that a larger fraction of the carbon is converted in the fuel reactor when more steam is used as the gasifying agent. This observation is consistent with the higher reactivity of steam-char gasification compared with CO_2-char gasification.

In addition to differences in gasification rates depending on the gasifying agent obtained in the TGA experiments, the inhibitory effect that the H_2 and CO in the FR atmosphere and the effect of particle size may have on gasification should also be taken into account. In Fig. 14, buckwheat husk showed the highest C_{AR} for all the biogenic residues in the gasification with steam despite the high reactivity of its char in the TGA tests. This apparent contradiction comes from the different conditions of both tests. In the TGA, small char particles were gasified under kinetic control, so the curves in Fig. 13 reflect the intrinsic reactivity of each char. In the fuel reactor, BW was fed as dense pellets (1254 kg/m^3, 10 mm in length), and the conversion of such large particles is limited by heat and mass transfer inside them: the gasifying agent cannot diffuse into the char as fast as it is consumed, and a high intrinsic reactivity makes this limitation more pronounced, because the reaction then takes place mainly near the outer surface of the particle. As a result, part of the BW char is transferred to the air reactor before it has been fully gasified, given the limited residence time of the solids in the fuel reactor.

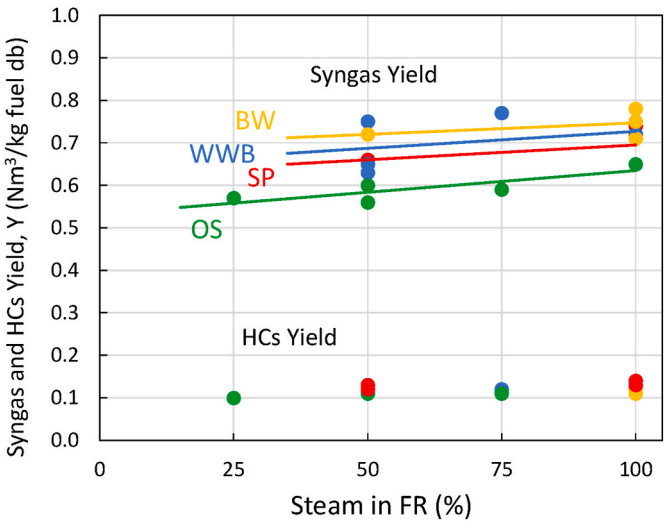


Fig. 15. Effect of the steam-to-CO_2 ratio (S/CO_2) on the syngas and hydrocarbon yield for the four biogenic residues. Conditions: λ ~0.3, T_{FR} = 950 °C.

Finally, the effect of the steam-to-CO_2 ratio (S/CO_2) on the syngas and hydrocarbon yield (Y_{sg} and Y_{HC}) was shown for the four residues in Fig. 15, considering only pellets of 10 mm length in the case of WWB and BW. Consistently with the weaker reactivity of CO_2, the syngas yield improved only slightly as the steam fraction increased, mainly because of the higher H_2 yield. Some differences were nevertheless found between fuels. Buckwheat husk reached the highest syngas yield of the four residues (≈0.8 Nm^3/kg biomass d.b.). Olive stone, in contrast, showed the lowest syngas yield of the four residues (≈0.65 Nm^3/kg biomass d.b.).

4. Conclusions

Chemical Looping Gasification of four European biogenic residues, representative of three different types of residues, was investigated to assess the influence of the biomass on the quality of the syngas obtained. Agricultural (olive stone, buckwheat husk pellets), forestry (spruce) and waste wood (waste wood type B) residues were successfully tested in a 20 kW_{th} CLG unit using ilmenite as oxygen carrier during about 85 h of steady-state operation. All residues presented similar composition regarding proximate and ultimate analyses. However, there were differences in their particle size and density. Thus, the effects of particle size and type of residue could not be fully separated in this campaign.

The oxygen-to-fuel ratio (λ) was confirmed as the most influential operating variable affecting the syngas quality, more than the temperature in the fuel reactor. Increasing λ raised the oxygen delivered to the fuel and oxidised a growing fraction of the H_2 and CO to H_2O and CO_2, whereas the CH_4 and C_2-C_3 fractions in the syngas remained essentially unaffected. The size of the CLG unit does not allow for its autothermal operation. At λ ≈ 0.30-0.35, the theoretical range estimated in the literature for autothermal operation, the syngas composition was remarkably similar for the four fuels, around 35 % H_2, 19 % CO, 36 % CO_2, 9 % CH_4 and 1 % C_2-C_3 (d.b.). Smaller biomass particles led to a lower carbon emission in the AR and a more oxidised syngas

composition, highlighting the importance of physical properties in addition to intrinsic fuel characteristics. At $\lambda \approx 0.30$-0.35, all types of biogenic residues reached similar syngas yield of approximately 0.7 Nm^3/kg biomass (dry basis) at 950 °C.

The choice of gasifying agent (steam or CO_2) was found to affect the syngas composition. Steam increased both hydrogen production and the H_2/CO ratio and reduced the carbon emitted in the AR, making it the preferred option for processes targeting hydrogen-rich syngas. In contrast, CO_2 can be used to tailor syngas composition for downstream applications requiring CO-rich mixtures, considering that its limited reactivity constrains its effectiveness as a conversion agent. Nevertheless, the trends obtained for the effect of λ, temperature and gasifying agent, provide a sound basis for the design and scale-up of CLG units and for the validation of reactor models.

The same batch of ilmenite was used throughout the entire experimental campaign (85 h of successive steady states). No agglomeration issues resulting from the interaction between biomass ash and the oxygen carrier were observed. However, longer experimental runs and a more detailed analysis of the used ilmenite particles are required to evaluate this aspect in greater depth.

CRediT authorship contribution statement

J.I. Ruiz Irizar: Writing – original draft, Investigation, Formal analysis, Data curation. **T. Mendiara:** Writing – review & editing, Resources, Methodology, Investigation, Data curation. **M.T. Izquierdo:** Writing – original draft, Resources, Methodology, Investigation, Data curation. **L.F. de Diego:** Writing – original draft, Resources, Methodology, Investigation, Data curation, Conceptualization. **F. García-Labiano:** Writing – review & editing, Supervision, Resources, Project administration, Investigation, Funding acquisition, Conceptualization.

Acknowledgements

This work has been supported by the European Union's Horizon Europe Research and Innovation Funding Programme under grant agreement No 101147737 (Bio-MeGaFuel). Views and opinions expressed are however those of the author(s) only and do not necessarily reflect those of the European Union or the European Climate, Infrastructure and Environment Executive Agency (CINEA). Neither the European Union nor CINEA can be held responsible for them.

Appendix A. Supplementary data

Supplementary data to this article can be found online at https://doi.org/10.1016/j.biombioe.2026.110267.

Data availability

Data will be made available on request.

References

[1] M. Millinger, F. Hedenus, E. Zeyen, F. Neumann, L. Reichenberg, G. Berndes, Diversity of biomass usage pathways to achieve emissions targets in the European energy system, Nat. Energy (2025) 226–242, https://doi.org/10.1038/s41560-024-01693-6.

[2] H.A. Alalwan, A.H. Alminshid, H.A. Aljaafari, Promising evolution of biofuel generations. Subject review, Renew. Energy Focus 28 (2019) 127–139, https://doi.org/10.1016/j.ref.2018.12.006.

[3] S.N. Naik, V.V. Goud, P.K. Rout, A.K. Dalai, Production of first and second generation biofuels: a comprehensive review, Renew. Sustain. Energy Rev. 14 (2010) 578–597, https://doi.org/10.1016/j.rser.2009.10.003.

[4] Y. Chisti, Biodiesel from microalgae, Biotechnol. Adv. 25 (2007) 294–306, https://doi.org/10.1016/j.biotechadv.2007.02.001.

[5] B. Abdullah, S.A.F. Syed Muhammad, Z. Shokravi, S. Ismail, K.A. Kassim, A. N. Mahmood, M.M.A. Aziz, Fourth generation biofuel: a review on risks and mitigation strategies, Renew. Sustain. Energy Rev. 107 (2019) 37–50, https://doi.org/10.1016/j.rser.2019.02.018.

[6] European Union, Directive (EU) 2023/2413 of the European Parliament and of the Council of 18 October 2023, 2023.

[7] Concawe/Imperial College London, Sustainable Biomass Availability in the EU to 2050, 2021.

[8] ICCT working paper 2021-39. https://theicct.org/wp-content/uploads/2021/12/eu-uk-biofuel-production-waste-nov21.pdf.

[9] S.Y. Searle, C.J. Malins, Waste and residue availability for advanced biofuel production in EU member states, Biomass Bioenergy 89 (2016) 2–10, https://doi.org/10.1016/j.biombioe.2016.01.008.

[10] F. Di Gruttola, D. Borello, Analysis of the EU secondary biomass availability and conversion processes to produce advanced biofuels: use of existing databases for assessing a metric evaluation for the 2025 perspective, Sustainability 13 (2021) 7882, https://doi.org/10.3390/su13147882.

[11] P. Ruiz, W. Nijs, D. Tarvydas, A. Sgobbi, A. Zucker, R. Pilli, et al., ENSPRESO - an open, EU-28 wide, transparent and coherent database of wind, solar and biomass energy potentials, Energy Strategy Rev. 26 (2019) 100379, https://doi.org/10.1016/j.esr.2019.100379.

[12] N. Hanchate, S. Ramani, C.S. Mathpati, V.H. Dalvi, Biomass gasification using dual fluidized bed gasification systems: a review, J. Clean. Prod. 280 (2021) 123148, https://doi.org/10.1016/j.jclepro.2020.123148.

[13] A. Goel, E.M. Moghaddam, W. Liu, C. He, J. Konttinen, Biomass chemical looping gasification for high-quality syngas: a critical review and technological outlooks, Energy Convers. Manag. 268 (2022) 116020, https://doi.org/10.1016/j.enconman.2022.116020.

[14] T. Mendiara, F. García-Labiano, A. Abad, P. Gayán, L.F. de Diego, M.T. Izquierdo, J. Adánez, Negative CO_2 emissions through the use of biofuels in chemical looping technology: a review, Appl. Energy 232 (2018) 657–684, https://doi.org/10.1016/j.apenergy.2018.09.201.

[15] I. Samprón, L.F. de Diego, F. García-Labiano, M.T. Izquierdo, Optimization of synthesis gas production in the biomass chemical looping gasification process operating under auto-thermal conditions, Energy 226 (2021) 120317, https://doi.org/10.1016/j.energy.2021.120317.

[16] B. Acharya, A. Dutta, P. Basu, Chemical-looping gasification of biomass for hydrogen-enriched gas production with in-process carbon dioxide capture, Energy Fuels 23 (2009) 5077–5083, https://doi.org/10.1021/ef9003889.

[17] A.L. Cerón, M.H.S. Baqain, O. Järvik, D. Nešumajev, A. Konist, Chemical looping gasification of biomass and mineral-rich oil shale fuel: opportunities for integrated valorisation and CO_2-Negative syngas, Biomass Bioenergy 209 (2026) 108972, https://doi.org/10.1016/j.biombioe.2026.108972.

[18] M. Greco-Coppi, X. Li, F. Marx, B. Arias, G. Grasa, A. Abad, F. Garcia-Labiano, T. Mattison, J. Ströhle, Recent advances in high-temperature solid looping processes toward commercial application, Int. J. Greenh. Gas Control 155 (2026) 104718, https://doi.org/10.1016/j.ijggc.2026.104718.

[19] G. Wei, F. He, Z. Huang, A. Zheng, K. Zhao, H. Li, Continuous operation of a 10 kW_{th} chemical looping integrated fluidized bed reactor for gasifying biomass using an iron-based oxygen carrier, Energy Fuels 29 (2015) 233–241, https://doi.org/10.1021/ef5021457.

[20] H. Ge, W. Guo, L. Shen, T. Song, J. Xiao, Biomass gasification using chemical looping in a 25 kWth reactor with natural hematite as oxygen carrier, Chem. Eng. J. 286 (2016) 174–183, https://doi.org/10.1016/j.cej.2015.10.092.

[21] O. Condori, A. Abad, M.T. Izquierdo, L.F. de Diego, F. García-Labiano, J. Adánez, Assessment of the chemical looping gasification of wheat straw pellets at the 20 kW_{th} scale, Fuel 344 (2023) 128059, https://doi.org/10.1016/j.fuel.2023.128059.

[22] O. Condori, A. Abad, F. García-Labiano, L.F. Diego, M.T. Izquierdo, J. Adánez, Parametric evaluation of clean syngas production from pine forest residue by chemical looping gasification at the 20 kW_{th} scale, J. Clean. Prod. 436 (2024) 140434, https://doi.org/10.1016/j.jclepro.2023.140434.

[23] O. Condori, A. Abad, M.T. Izquierdo, L.F. Diego, I. Funcia, R. Pérez-Vega, et al., Effect of biomass torrefaction on the syngas quality produced by chemical looping gasification at 20 kW_{th} scale, Energy Fuels 38 (2024) 11779–11792, https://doi.org/10.1021/acs.energyfuels.4c01096.

[24] P. Dieringer, F. Marx, F. Lebendig, M. Müller, A. Di Giuliano, K. Gallucci, et al., Fate of ilmenite as oxygen carrier during 1 MW_{th} chemical looping gasification of biogenic residues, Appl. Energy Combust. Sci. 16 (2023) 100227, https://doi.org/10.1016/j.jaecs.2023.100227.

[25] F. Marx, P. Dieringer, J. Ströhle, B. Epple, Process efficiency and syngas quality from autothermal operation of a 1 MW_{th} chemical looping gasifier with biogenic residues, Appl. Energy Combust. Sci. 16 (2023) 100217, https://doi.org/10.1016/j.jaecs.2023.100217.

[26] Z. Li, J. Li, Y. Wang, W. Li, G. Wei, X. Liu, S. Lin, Q. Sun, Y. Yang, A. Zhao, et al., Demonstration of biomass chemical looping gasification in a 5 MW_{th} pilot unit using ilmenite as oxygen carrier, Fuel 405 (2026) 136472, https://doi.org/10.1016/j.fuel.2025.136472.

[27] V. Skrabanja, I. Kreft, T. Golob, M. Modic, S. Ikeda, K. Ikeda, et al., Nutrient content in BuckWheat milling fractions, Cereal Chem. 81 (2004) 172–176, https://doi.org/10.1094/CCHEM.2004.81.2.172.

[28] G. Rodríguez, A. Lama, R. Rodríguez, A. Jiménez, R. Guillén, J. Fernández-Bolaños, Olive stone an attractive source of bioactive and valuable compounds, Bioresour. Technol. 99 (2008) 5261–5269, https://doi.org/10.1016/j.biortech.2007.11.027.

[29] K. Borzęcki, R. Pudełko, M. Kozak, M. Borzęcka, Antoni Faber, spatial distribution of wood waste in Europe, Sylwan 162 (7) (2018) 563–571, https://doi.org/10.26202/sylwan.2018008.

[30] N. Scarlat, M. Martinov, J.F. Dallemand, Assessment of the availability of agricultural crop residues in the European Union: potential and limitations for bioenergy use, Waste Manag. 30 (2010) 1889–1897, https://doi.org/10.1016/j.wasman.2010.04.016.

[31] A.A. Rentizelas, A.J. Tolis, I.P. Tatsiopoulos, Logistics issues of biomass: the storage problem and the multi-biomass supply chain, Renew. Sustain. Energy Rev. 13 (2009) 887–894, https://doi.org/10.1016/j.rser.2008.01.003.

[32] O. Condori, F. García-Labiano, L.F. de Diego, M.T. Izquierdo, A. Abad, J. Adánez, Biomass chemical looping gasification for syngas production using ilmenite as oxygen carrier in a 1.5 kW_{th} unit, Chem. Eng. J. 405 (2021) 126679, https://doi.org/10.1016/j.cej.2020.126679.

[33] A. Abad, J. Adánez, A. Cuadrat, F. García-Labiano, P. Gayán, L.F. de Diego, Kinetics of redox reactions of ilmenite for chemical-looping combustion, Chem. Eng. Sci. 66 (2011) 689–702, https://doi.org/10.1016/j.ces.2010.11.010.

[34] I. Samprón, L.F. de Diego, F. García-Labiano, M.T. Izquierdo, J. Adánez, Influence of oxygen carrier on CH4 reforming reaction linked to biomass chemical looping gasification process, Energy Fuels 36 (2022) 9460–9469, https://doi.org/10.1021/acs.energyfuels.2c00705.

[35] A. Abad, P. Gayán, R. Pérez-Vega, F. García-Labiano, L.F. de Diego, T. Mendiara, M.T. Izquierdo, J. Adánez, Evaluation of different strategies to improve the efficiency of coal conversion in a 50 kW_{th} chemical looping combustion unit, Fuel 271 (2020) 117514, https://doi.org/10.1016/j.fuel.2020.117514.